Journal of Materials Chemistry B

Accepted Manuscript

This is an *Accepted Manuscript*, which has been through the Royal Society of Chemistry peer review process and has been accepted for publication.

Accepted Manuscripts are published online shortly after acceptance, before technical editing, formatting and proof reading. Using this free service, authors can make their results available to the community, in citable form, before we publish the edited article. We will replace this *Accepted Manuscript* with the edited and formatted *Advance Article* as soon as it is available.

You can find more information about *Accepted Manuscripts* in the Information for Authors.

Please note that technical editing may introduce minor changes to the text and/or graphics, which may alter content. The journal's standard Terms & Conditions and the Ethical guidelines still apply. In no event shall the Royal Society of Chemistry be held responsible for any errors or omissions in this *Accepted Manuscript* or any consequences arising from the use of any information it contains.

ROYAL SOCIETY OF CHEMISTRY

www.rsc.org/materialsB

Journal of Materials Chemistry B

ARTICLE

Polycaprolactone Fibers with Self-Assembled Peptide Micro/ Nanotubes: a Practical Route Towards Enhanced Mechanical Strength and Drug Delivery Applications

Received 00th January 20xx,
Accepted 00th January 20xx

DOI: 10.1039/x0xx00000x

www.rsc.org/

M. S. Liberato,[a] S. Kogikoski Jr.,[a] E. R. da Silva,[a] D. R. Araújo,[a] S. Guha,[b] and W. A. Alves[a,*]

Peptide-based scaffold is frontier research in materials science with widespread impact in biomedical engineering. In this paper, we describe a hybrid material formulated through the conjugation of electrospun polycaprolactone (PCL) fibers and micro/nanotubes of L,L-diphenylalanine (FF-MNTs). Morphology and crystallinity in the composite matrices are investigated by a wide range of analytical techniques including electron microscopy, thermal analyses, X-ray diffraction and micro-tomography. Peptide assemblies are found to produce deep modifications on microstructure of PCL fibers, impacting average diameters, crystallinity degree and porous size in the polymer network. These changes are correlated with mechanical properties of the resulting scaffolds, whose strength is found to exhibit a brittle-to-ductile transition upon increasing of FF-MNTs and lead to enhanced Young's modulii of polymer fibers. The PCL/FF-MNTs composites were tested for drug delivery application of a lipophilic drug, benzocaine. *In-vitro* permeation studies have shown that these polymer/peptide hybrids are able to produce steady release of benzocaine over periods up to ~ 13 hours, much higher than commercially available gel formulations. Enzymatic tests have shown significant increment on biodegradation rates in PCL/FF-MNTs hybrids containing higher peptide amounts, which exhibited almost 100% of weight loss against only 10% found in pure PCL. Our findings indicate that PCL/ FF-MNTs materials are a simple route towards enhanced mechanical strength of PCL networks, able to promote controlled drug delivery from a completely biodegradable matrix.

1. Introduction

Polymer-based skin patches for drug delivery applications should be malleable, hydrophilic and have a slow uptake of the drug in the body.[1,2] However, the non-trivial balance of mechanical and thermal properties often required for attaining these characteristics represents a major challenge toward the full exploitation of these functional materials.[1,3,4] Designing nanocomposites with the addition of organic or inorganic self-assembled nanostructures into polymeric matrices is a promising strategy to overcome this drawback.[5] Bio-inspired self-assemblies such as L,L-diphenylalanine micro/nanotubes (FF-MNTs) are suitable for designing nanocomposite materials due to their excellent mechanical strength (19 GPa),[6,7] thermal degradation stability (up to 200 °C), and resistance to disassembly in either organic solvents or water.[8] Moreover, the aggregation process may be controlled and lead to different morphologies, which may contribute to a better dispersion and more cohesive interaction with different polymeric materials.[9,10]

Although several reports are available on the usage of self-assembled nanostructures for enhancing mechanical strength in nanocomposites, detailed studies on peptide-based scaffolds incorporated into polymer matrices, remain relatively scarce in literature.[11] Recently, FF-MNTs were used as reinforcement agent in an epoxy matrix prepared by solvent casting method.[12] The incorporation of these structures has led to impressive growth of shear strength, whereas thermal and elongation properties of the epoxy polymer have been found to remain preserved.[12] Other studies have investigated the self-assembling of cyclic peptides into poly-D,L-lactide (PDLLA) solutions, and found the formation of peptide microcrystals suitable for increasing the stiffness and Young's modulus of the hybrid composites.[13] In addition, fibers based on a block copolymer of biotin-poly-(ε-caprolactone) prepared by electrospinning have been used as template for promoting spatial organization of biomolecules within the electrospun material.[14] Interestingly, this material has shown a dynamic gradient of the arranged biomolecules reproducing gradient conditions found in biological tissues.[14]

The FF-MNTs were already evaluated as potential vehicles for drug delivery using a model compounds as to mimic a drug.[15] It has been found that FF-MNTs are able to modulate the release of the load, indicating their ability to deliver drugs at constant rates in the body. Cytotoxicity investigations revealed high cell viability up to concentrations of 5 mg mL^{-1}, demonstrating the low toxicity and potential biocompatibility of FF-MNTs. On the other hand, poly-ε-caprolactone (PCL) is a very

[a] Centro de Ciências Naturais e Humanas, Universidade Federal do ABC, 09210-580, Santo André, SP, Brazil.
[b] Department of Physics and Astronomy, University of Missouri, Columbia, Missouri 65211, United States
* e-mail: wendel.alves@ufabc.edu.br

Electronic Supplementary Information (ESI) available: more SEM, Micro-CT and Mechanical Properties data. See DOI: 10.1039/x0xx00000x

Journal of Materials Chemistry B Accepted Manuscript

Please do not adjust margins

attractive material widely investigated for biomedical applications.[16-19] Nevertheless, the proper designing of scaffolds for drug delivery often needs the addition of compatibilizers, which change the chemical characteristics and plays an indirect role on the mechanical characteristics, crystallinity, solubility, and degradation behaviours. Unfortunately, these changes on the finer chemistry of the matrix usually lead to significant loss of properties suitable for drug delivery.[19-21]

In this work, we design an inedited peptide-based composite built up from the conjugation between FF-MNTs and PCL. Peptide and polymer were co-solubilized and undergone electrospinning for producing fibers with controlled tensile properties. We found that addition of FF into fibrous PCL significantly enhances the elastic modulus in the electrospun scaffolds. This approach has created stronger fibers with lengths reaching the micrometer scale and only a few hundred nanometers in diameter. Scaffolds exhibit porous morphology with diameters ranging from 360 to 570 nm, depending on the peptide amount in the matrix. Differential scanning calorimetry (DSC) and X-ray powder diffraction (XRPD) shows that the microstructure of the polymeric matrices are strongly affected by the presence of FF-MNTs, with important consequences on the elastic behaviour of the hybrid material. The potential of these scaffolds for controlled drug release is demonstrated using a lipophilic anaesthetic, benzocaine (BZC), as load. The resulting network, with interconnected pores across the polymer matrix, is suitable for drug delivery applications and exhibits good biodegradability properties. X-ray microtomography (micro-CT) clearly shows reduction on porosity upon addition of FF-MNTs, which has been interpreted as an advantage for producing membranes for steady release of the drug load.

2. Experimental Section

2.1. Materials

All reagents used in the experiments had analytical purity. Chloroform, methanol and sodium azide were purchased from Synth (Brazil). Alcohol 1,1,1,3,3,3-hexafluoro-2-propanol (HFP), L,L-diphenylalanine (FF), poly-(ε-caprolactone) (PCL) (Mw:70.000 - 90.000) and proteinase-K were purchased from Sigma-Aldrich (USA) and used without further purification.

2.2. Preparation of FF-PCL composites

Polymer fibers were obtained by electrospinning organic solutions containing FF and PCL. Lyophilized L,L-diphenylalanine (FF) powder was dissolved into 1,1,1,3,3,3-hexafluoro-2-propanol (HFP) and further added to PCL solutions prepared into chloroform/methanol mixtures (1:3 v/v). The mass percentage of polymer in the solution was kept at 8.0 wt%, whereas peptide/PCL ratios ranged from 2.5% to 50%. Co-solubilization was attained upon continuous stirring over a period of 2 hours at room temperature. The mixtures were transferred to 15 mL syringes with 12G needles. Syringes were placed at vertical position and dripping flow was obtained by gravity. Square 15 × 15 cm² plates, covered with aluminum foils, were positioned at 15 cm from the needles and a voltage of 22 kV was established for spinning fibers. Collection time was of about 4 hours.

2.3. Electron Microscopy Analyses

Scanning electron microscopy images from composite membranes were obtained on a high-resolution JSM 6330F instrument (SEM-FEG), at the Center for Research in Energy and Materials (CNPEM, Campinas, Brazil). Secondary electrons were collected after back scattering from Au-coated samples hit by electron beams with energy 5 kV.

2.4. X-Ray Powder Diffraction

Diffraction experiments were conducted at the XRD1 beamline at the Brazilian National Synchrotron facility (LNLS, Campinas, Brazil). Photons energy was set at 10 KeV and counting rates were adjusted at 1×10^7 photons s^{-1}. The beam had rectangular cross section with dimensions 2 × 0.2 mm² and a Mythen 1K strip detector, composed of 1280 channels with 50 microns each, was used to record the data. The angular range was scanned in the interval $10° < 2\theta < 30°$, with steps of 0.005°. Calibration was performed using Al_2O_3 standards and instrumental broadening was estimated at $\Delta 2\theta \sim 0.04°$. The set up was mounted in transmission mode and polymer membranes were conveniently placed on metallic grids.

2.5. X-ray micro-tomography

X-ray micro-CT measurements were performed using a Bruker SkyScan 1272 instrument. The X-ray source operated at voltage of 20 KV and current of 175 μA. Data were recorded by a 2D X-ray detector with 16 Megapixels, pixel size of 3.37 μm. Specimens with dimensions 8.5 × 0.2 × 0.14 mm³ were positioned along the vertical axis of a goniometer and rotated at angular steps of 0.4°. In this configuration, a z-resolution of about 350 was achieved and 450 images were acquired to cover an angular range of 180°. Image treatment and 3D reconstructions were performed using the manufacturer softwares DataViewer and CTVox. The porosity was measured using CTAn software (SkyScan, Bruker microCT), with selected voxel coefficient.

2.6. Mechanical analyses

Mechanical analyzes were performed using samples with dimensions 12.9 × 6.3 × 0.12 mm³ using a Dynamic Mechanical Analyzer (DMA) - TA Instruments (DMA Q800) in extension mode. Stress × strain curves were obtained using displacement rates of 700 μm min^{-1} (ASTM D882).

2.7. Differential Scanning Calorimetry

Differential Scanning Calorimetry (DSC) assays were performed on a TA Instruments DSC Q-series apparatus. Samples were first heated from room temperature up to 40°C, then cooled down to -90°C. In the following, they were heated to 220°C and cooled down to -65°C. Data exhibited in Figure 2 (and SI file) have been recorded during this second heating/cooling cycle. Temperature rate of 10° C min^{-1} was used throughout the experiments, which were performed under nitrogen atmosphere.

2.8. *In vitro* permeation assays

In vitro permeation assays were performed using vertical Franz-type diffusion cells with 0.6 cm^2 (Vidrotec®, Porto Alegre-RS, Brazil) with artificial membranes (nitrocellulose sheets, 0.05 μm pore size) impregnated with isopropyl myristate to simulate

Journal of Materials Chemistry B Accepted Manuscript

This journal is © The Royal Society of Chemistry 20xx

Please do not adjust margins

hydrophobicity of stratum corneum[22] under occlusive (vapor-permeable) conditions. The donor compartment was filled with 1.0 g of the formulations and the receptor compartment with 5 mM Hepes buffer containing a 0.9% NaCl solution, pH 7.4, at 32.5 ºC under constant magnetic stirring (350 rpm). At predetermined time intervals, aliquots from the receptor compartment were analyzed by UV-VIS spectrophotometry to quantify the released drug content. Analysis was performed by using a calibration curve obtained previously (y = - 0.07881 + 0.2306X, R^2 = 0.9989, limit of quantification 0.009 μg.mL^{-1} and limit of detection = 0.053 μg.mL^{-1}). Data were expressed as percentage or mean ± sd and undergone to one-way ANOVA with post hoc Tukey-Kramer test using Graph Pad Instat (Graph Pad Software Inc., USA) or Origin 6.0 (Microcal™ Software, Inc., Northampton, MA, USA) programs. Statistical differences were defined as $p < 0.05$.

2.9. Biodegradability

Composite membranes were weighted before incubation at 37 °C in tris-HCl 0.05 mol L^{-1} (pH 8.6) buffer solution containing 1.0 mg proteinase-K enzyme and 0.02% sodium azide. The buffer/enzyme solution was monitored over 25 hours. At time intervals of 2 hours, the membranes were removed from the solution, washed, vacuum dried and then weighed. The percentage of weight loss was obtained just by computing the mass loss over the initial mass using the expression $[(m_{after}-m_0)/m_0]\times100$, where m_{after} is the vacuum dried weight and m_0 is the initial weight of each sample.

3. Results and Discussion

3.1. Morphology investigation

Scanning electron micrographs from peptide/PCL samples, Figure 1, show the formation of uniform fibers homogeneously distributed across the surface of aluminum foils used as a substrate for collection during electrospinning (additional images in the SI file, Figure S1). One observes randomly oriented fibers, with lengths reaching micrometer scale, and thickness ranging from ~360 nm to ~570 nm, consistently forming networks with nonwoven fabric-like features. Interestingly, the general morphology of PCL fibers does not change upon addition of FF; however, their diameters are found to consistently decrease as the amount of peptide is incremented in the matrix (see Table S1). These findings could be tentatively ascribed to electrostatic attraction between polymer and peptides, which potentially hinders association between PCL fibrils and suppress the growth of larger structures. Additionally, charges in the solution during jet formation may interact with the external electric field, stretching the fibers and thus reducing the diameters.[23]

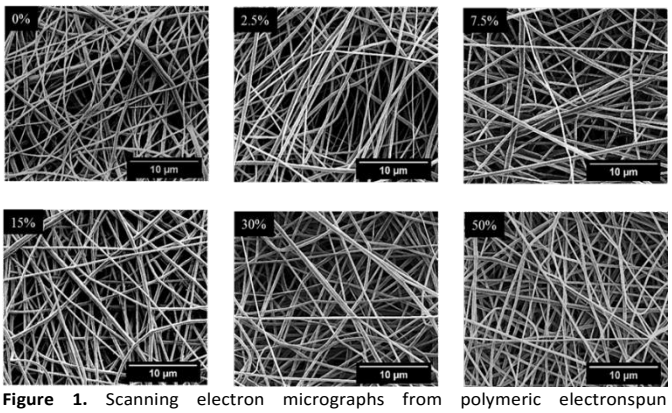

Figure 1. Scanning electron micrographs from polymeric electronspun membranes at different FF/PCL percentages.

To get deeper insight into the role of self-assembled FF in the composite structure, we heated the polymer networks up to 180°C, under controlled atmospheric conditions. The heating temperature was chosen to be much higher than PCL melting point (~60°C), but well below FF degradation temperature (~220 °C).[8, 24, 25] Changes in sample morphology are clearly observed in comparison with the non-heat treated films (see Figure S2). The polymer appears aggregated and forms an amorphous melted phase whereas FF-MNTs remain stable. These findings are a strong indicator that the polymer behaves as template guides for the peptide self-assembly and FF nanotubes remain mostly hosted within polymer fibers, forming a core-shell architecture. In addition, the systematic absence of FF-MNTs in the interstice of polymer network supports the incorporation of peptide assemblies in the core of the fibers. Since the size of the fibers can be managed by controlling the electrospinning parameters such as voltage, flow rate and peptide/polymer ratio, this strategy has a great potential for templating and synthesizing these hybrid scaffolds incorporating peptides.

3.2. DSC and XRPD Assays.

Differential scanning calorimetry (DSC) and X-ray powder diffraction (XRPD) have been performed to probe intermolecular interactions and assess how peptides affect the semi-crystalline nature of the PCL matrix. As discussed further, these data have been crucial to correlate striking changeovers on mechanical properties of the hybrid materials and ordering state of polymer chains. In Figure 2, thermograms from samples containing different FF/PCL ratios are shown. Thermal parameters arising from these assays – namely, crystallization and melting temperatures, enthalpies, entropies and crystallinity degree - are exhibited in Table 1.

Thermograms are characterized by exothermic (Fig. 2A) and endothermic peaks (2B), respectively, corresponding to crystallization and melting processes in the polymer phase.[26, 27] In samples containing higher FF amounts, endothermic peaks are also observed around 160 °C (pointed by black arrows in Fig. 2B), which has been ascribed to hexagonal-to-orthorhombic transitions into the crystalline structure of FF-MNTs.[28-30] Focusing on the thermal behaviour associated to the polymer phase, one observes that crystallization temperature is found at T_c = 22 °C in bare PCL matrices whereas composites exhibit an impressive jump with T_c increasing up to 33 °C in FF-containing samples (see Fig. 2A). In contrast, melting temperatures apparently are not strongly affected by peptide species and remain stable around T_m = 61.2 ± 1.3 °C (Fig. 2B). However, more

Journal of Materials Chemistry B Accepted Manuscript

Table 1. Thermal parameters and crystallinity degrees arising from DSC analyses.

FF/PCL ratio (%)	T_c (°C)	ΔH_c ($J \cdot g^{-1}$)	T_m (°C)	ΔH_m ($J \cdot g^{-1}$)	ΔS_m ($J \cdot °C^{-1} \cdot g^{-1}$)	X_c (%)
0	22	49.5	61	64.4	0.19	48
5	31	45.1	60	53.3	0.16	41
10	33	44.1	63	49.2	0.15	40
30	31	37.5	62	39.7	0.12	38
50	33	33.5	60	29.9	0.09	33

remarkable changes in the thermal behaviour of the composites are related to crystallization/melting enthalpies. In fact, one observes monotonic decreasing on specific enthalpies associated either to exothermic or to endothermic transitions (see Table 1).

Crystallization enthalpy is found to decrease from ΔH_c = 49.5 $J \cdot g^{-1}$ in bare PCL down to ΔH_c = 33.5 $J \cdot g^{-1}$ in the 50% (FF/PCL) sample. Similarly, melting enthalpy decreases from ΔH_m = 64.4 $J \cdot g^{-1}$ to ΔH_m = 29.9 $J \cdot g^{-1}$. These findings indicate that the presence of FF species in the interstice of the polymer phase likely weakens the strength of inter-chain interactions, directly affecting the crystalline behaviour as suggested by the broadening of endothermic peaks. To quantify these modifications, we have used the enthalpy data listed in Table 1 to calculate the crystallinity degree in our samples through the relationship: $X_c(\%) = [\Delta H_m/(w \times \Delta H_m^{\infty})] \times 100$, where ΔH_m^{∞} is the heat of fusion for 100% crystalline PCL (here, assumed to be ΔH_m^{∞} = 135 $J \cdot g^{-1}$)[31] and w is the weight fraction of polymer in the sample. The degree of crystallinity obtained from the thermal data is found to decrease from X_c = 48 %, in the pure PCL formulation, to about X_c= 33% in the sample formulated with 50% FF/PCL. This finding is consistent with loss of ordering arising from weaker interactions between polymer chains.

Entropic contributions also play an important role in the FF/PCL composites described here. To estimate entropy gain in different samples, we have determined heat capacity (C_p) as a function of temperature (SI file, Figure S3). Formulations containing FF clearly exhibit higher C_p values when compared to pristine PCL. Plots of $C_p/T \times T$, integrated in the range between 0°C and 30°C, reveal strong entropy gain and attest that higher amounts of peptide lead to higher levels of disorder in the mixtures (see SI file for details). This behaviour is likely a consequence of mixing entropy which appears in the system upon addition of peptides to the formulations. Furthermore, it could be also correlated to growth of configurational entropy of polymer chains, which is consistent with diminution of crystallite sizes revealed by X-ray assays (see below).

Entropies of fusion, ΔS_m, also have been estimated. At the melting point, equilibrium is reached and Gibbs free energy change is null: $\Delta G_m = \Delta H_m - T \times \Delta S_m = 0$. To a first approximation, we have assumed $T = T_m$ throughout the melting process

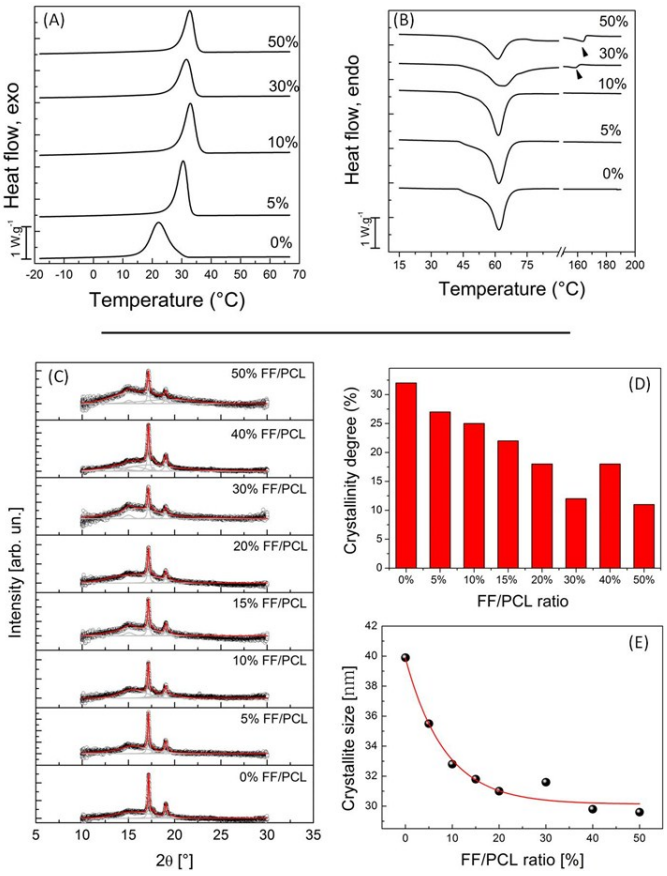

Figure 2. Top: DSC scans from FF/PCL samples showing heat flows associated to (A) crystallization and (B) melting of PCL chains. Black arrows in (B) indicate phase transitions associated to peptide self-assemblies hosted in the interstice of the polymer matrix; bottom: (C) synchrotron X-ray powder diffraction patterns from PCL matrices containing peptides at the indicated FF/PCL percentages. Gray lines: Gaussian functions used for deconvoluting Bragg peaks and diffuse (amorphous) scattering, red lines are the summation of deconvoluted functions; (D) crystallinity degree obtained from XRPD; (E) crystallite size calculated from the most intense Bragg peak (110), see text for details.

and then ΔS_m values could be calculated straightforward by using ΔH_m and T_m data obtained previously. Estimations for ΔS_m are listed in Table 1 and they reveal that entropy of fusion decreases upon increasing of peptide in the mixture. This result is in line with higher levels of disorder found in the solid phase of FF/PCL composites. In fact, since crystallinity is lower when FF is present in the polymer matrix, the entropy gain needed for fusion presumably should be lower.

To further understand, the structure of our peptide/polymer composites and obtaining independentmeasurements on crystallinity degree, we have performed synchrotron XRPD experiments. Furthermore, these assays have allowed us to quantify the crystallite size in the samples. Data from these measurements are shown in Fig. 2C, where one observes that diffractograms are dominated by intense Bragg peaks at 2θ ~ 17.2° and ~ 19.1°, accompanied by shallow shoulders at 17.7° and 19.5°C. These reflections, in increasing angular order, are attributed to the Miller indexes (110), (111), (200) and (201) of an orthorhombic unit cell with a = 7.55 Å, b = 4.97 Å and c = 17.27 Å, in close agreement with previous literature which has found that PCL chains are

Journal of Materials Chemistry B Accepted Manuscript

This journal is © The Royal Society of Chemistry 20xx

Please do not adjust margins

organized into a $P2_12_12_1$ space group.[31] Additionally, a broad peak centered at 2θ ~15° (011) appears convoluted with the diffuse contribution of the amorphous PCL phase, which increases upon FF addition likely due to weakening of intermolecular interactions in the matrix. The crystallinity degree from XRPD data was obtained by considering the ratio between the areas under the Bragg peaks and the total scattering across the angular range (including the amorphous phase). Contributions from both Bragg peaks and diffuse scattering have been deconvoluted by adjusting Gaussian functions and the corresponding areas have been calculated (see gray lines in Figure 2C). In Figure 2D, we show crystallinity degrees arising from this procedure where a decrease in crystallinity is observed upon peptide addition, in agreement with the general trend found on DSC data (Table 1). In addition, we observe that crystallinity values estimated from PXRD data are lower than those estimated from DSC assays did. This behaviour has been also observed elsewhere [31] and it is ascribed to partial crystallization of amorphous polymer during heating/cooling cycles which contribute for increasing the degree of ordering on DSC experiments. In addition, since our samples have fibrillar structures, the presence of anisotropy in our membranes potentially leads to underestimation of crystallinity obtained from X-ray assays. Crystallite sizes have been calculated from the most intense reflection (110) by using the Scherrer equation:[32] $t = (0.9 \times \lambda)/(\beta \times \cos\theta)$, where t is the crystallite size, λ is the X-rays wavelength and β is the full width at maximum half (FWHM) of the Bragg peak centered at angle θ. Overall, one observes that the size of the crystalline domains decreases upon increasing of FF in the formulation, dropping from t ~ 35.5 nm, in the pure PCL matrix, to t ~ 29.5 nm in the formulation containing the highest amount of peptides.

In light of the structural data described above, we propose two mechanisms by which the crystalline behavior of PCL is affected by peptides in our composites. A first hypothesis arises from dispersing FF monomers into PCL matrix, which potentially reduces cross-linking efficiency in polymer network. In this case, FF molecules could introduce a competition for H-bonding between peptide end groups and oxygen sites along PCL chains, leading to lower chain-chain interactions. A second mechanism could be related to the interphase formed in the vicinities of FF-MNTs/PCL interfaces. In this scenario, higher availability of FF assemblies likely increases the volume of the interphase, exhibiting properties different from those observed in the bulk, and thus contributing to change the average behavior of the matrix FF-MNTs/PCL.

3.3. Mechanical Properties and X-ray Micro Tomography Measurements

Tensile tests were carried out for samples with formulations ranging from 2.5% to 50% (FF/PCL mass ratio). Results arising from these assays are shown in Figure 3A.

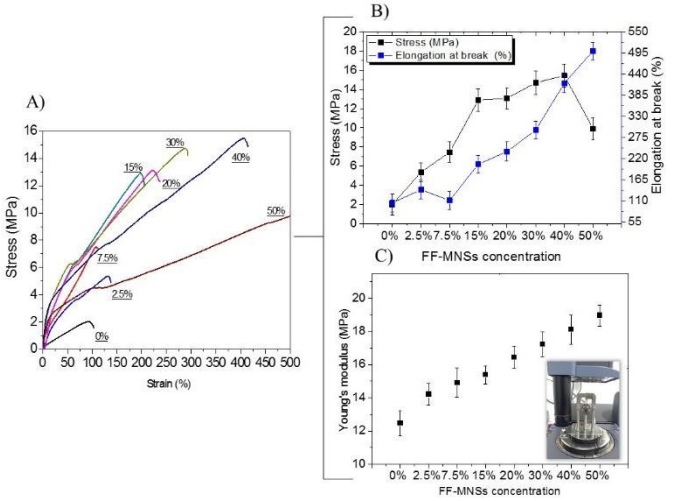

Figure 3. (A) Stress–strain curves from electrospun samples; (B) Stress and elongation at break behaviour upon peptide concentrations in the formulations; (C) Young modulus for the different peptide concentrations.

The stress-strain curves contain information about strain and stress limits, Young moduli and elongations at break. Elongation at break for samples containing 2.5% and 7.5% FF-MNTs are similar to pure PCL, whereas stress values are found to strongly increase even same elongation. For FF amounts higher than 7.5%, stress at break increases from 2 MPa to a steady value of ~14.5 MPa. Similarly, elongation at break increases from ~ 100% to ~ 400%, indicating that the composites become more flexible. We evaluate these values from Figure 3B and the results are listed in Table S2. One observes that Young modulus, maximum tensile strain and elongation at break are greatly improved, showing overall enhancement of mechanical properties (mainly flexibility) upon addition of FF-MNTs to PCL matrix. For instance, Young modulus increased from 12.5 MPa, in bare PCL, to a maximum of 18.1 MPa in formulations with 50% FF/PCL ratio (see Figure 3C).

Dispersion, orientation and cohesion of the FF-MNTs within the matrix likely impact mechanical properties of the composites. A net effect of different interactions at play during electrospinning of our polymer solutions- hydrogen bonds, π-stacking, hydrophobic interactions – improve elastic properties upon increasing of FF-MNTs in the sample. We hypothesize that this finding results from a better dissipation of the applied forces across the network.[12, 33] At lower amounts of FF-MNTs, elongation behaviour of the hybrid material is dominated by PCL characteristics – i.e., mechanical properties of the composite are closer to those found in peptide-free PCL. However, even at low FF concentrations, peptides and polymer interact to enhance stress at break, which could eventually be ascribed to the intercalation of FF monomers in the interstice of the polymer phase. Increasing the peptide concentration – and thus the amount of FF-MNTs in the composite - until 40% makes FF-MNTs to coalesce, forming larger peptide-containing domains in the composite (as evidenced in SI file, Figure S2). These domains interact strongly with the amorphous region of the PCL, making it harder to break. The composite with 50% of

Journal of Materials Chemistry B Accepted Manuscript

Please do not adjust margins

FF-MNTs becomes very ductile to the extent that it is not possible to break the material in the strain range used in our experiments. In this case, mechanical properties in the higher concentration composites are strongly influenced by FF-MNTs. exhibiting characteristics which are very distinct compared to bare PCL.[33]

Generally, matrices that are reinforced and oriented exhibit improved strength when tensile forces are applied parallel to the orientation axis.[34] Here, in despite membranes apparently are made up from randomly-distributed networks, a similar behaviour has been observed. We tentatively propose that this effect originates from a partially oriented system. In fact, although the electrospinning process leads to a random dispersion of the fibers onto the substrate (see microscopy images); the applied electric field interacts with dipole moment of FF molecules. In this case, such interaction possibly induces partial orientation of the polymeric fibers, which could exhibit some degree of local ordering and improve the mechanical properties as peptide concentration rises (see Figure 4B).

X-ray micro tomography (Micro CT) yields insights into the internal structure of the scaffolds. It is a non-invasive technique using an incident X-ray beam at different scan angles, sectioning the object into 2D images, which are further combined for retrieving 3D reconstructions. Micro-CT is able to provide information about porosity and allows for estimating empty space in the samples. Porosity measurements were performed on ~500 slices in volume for all concentrations. The 2D images show changes in the distribution of pores into polymeric matrices upon increasing of the concentration of FF-MNTs.

Figure 4A shows cross-section micro-CT images from representative formulations (see SI file, Figure S4, for additional images from all formulations). The contrast effect observed in the images (yellow, white and blue colors) is based on different absorption of X-rays and how they reflect different composition domains in the samples. Vacancies (black color) decrease as the concentration of FF-MNTs increases, attesting that pores in the matrix are filled by polymer.

Micro-CT data also shed light on the shape and alignment across the polymer network. Pure PCL fibres exhibited higher tendency to form globular clusters when compared to the composites. In contrast, addition of FF-MNTS resulted in higher alignment of the fibres, as schematically shown in Figure 4B. In Figure 4C, average porosity values obtained from micro-CT images are plotted as a function of the peptide amount in the matrix. In agreement with the behaviour exhibited by crystallinity degree, and crystallite size derived from thermal and XRPD analyses, one observes porous sizes also decay with increasing peptide in the composite. These findings show that structural changes occurring at the supramolecular level are reflected at the microscopic structure of the samples and ultimately leads to enhanced elastic properties.[34]

3.4. *In Vitro* Permeation Studies

In vitro permeation studies were performed for all composite formulations (with 10%wt BZC) in comparison to a commercial available gel formulation (20% BZC). Figure 5A shows the behavior of the drug release curves from 30 minutes to 24 hours. The results from in vitro permeation profiles were plotted considering the permeation rate against time. The commercial gel formulation showed higher BZC permeated concentration compared to FF-MNTs/PCL scaffolds. Furthermore, the BZC permeation rate from films was reduced upon increasing the FF concentration (Figure 5B); presumably, a consequence of the lower porosity observed in these complexes. After 24 h, the BZC permeation rates from samples containing 7.5, 15, and 30% FF were statistically different from that observed for the commercial gel and 2.5% FF ($p<0.05$). These results suggest that the slow BZC permeation rate can be attributed to the possible interaction of the hydrophobic ester-type local anesthetic BZC with the polymeric networks (in special hydrophobic polymers, such as PCL) on films. We observed similar results of release based on the FF-MNTs concentration. Samples containing higher concentrations promoted a slower release rate compared to the common gel. The release profiles were fitted by exponential functions to obtain the rate constant as a function of the peptide concentration. The common gel presented a lag time of ~0.5 hours while it was gradually increased from 6.6 to 13.3 hours for FF concentrations from 2.5% to 15%. The differences in the percentage concentration of BZC in the common gel (20%) and the membrane (10%) may explain the differences in the lag time values. Even for the membranes that have a lower

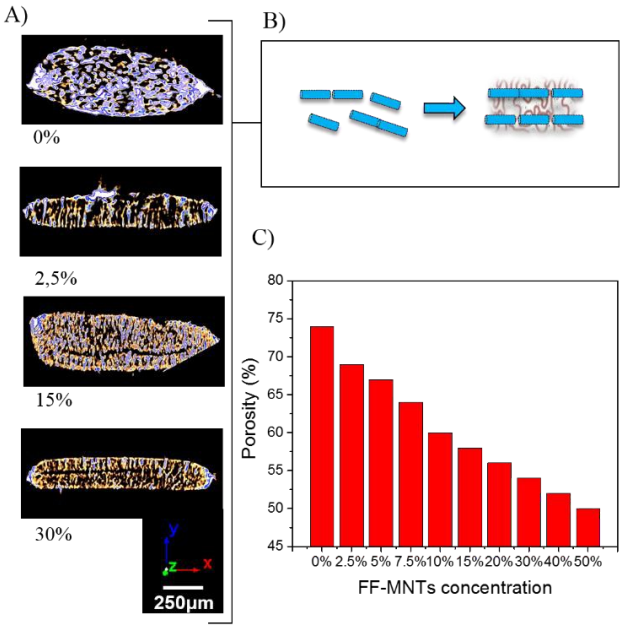

Figure 4. Microtomography analyses from FF-MNTs/PCL samples. (A) Representative slices showing the inner morphology of the membranes, exposing the porous network; (B) Schematic representation for the proposed organization framework where the presence of FF-MNTs induces local ordering on polymer network reinforcing its mechanical properties. The blue tubes denote the PCL fibers. (C) Porosity of the membranes obtained from the distribution of pores for ~500 slices.

Journal of Materials Chemistry B Accepted Manuscript

This journal is © The Royal Society of Chemistry 20xx

Please do not adjust margins

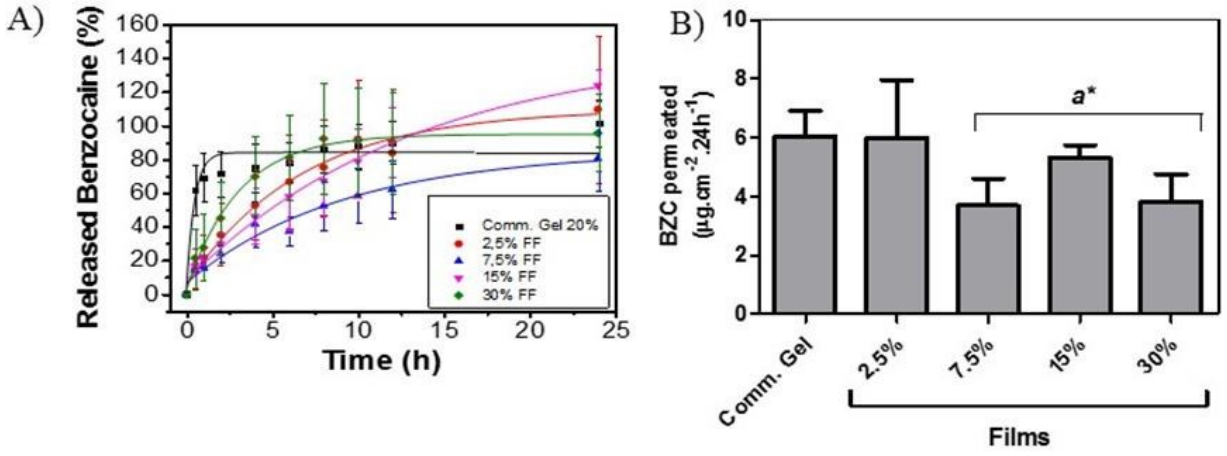

Figure 5. (A*)* Release curves of BZC obtained by UV-Vis spectrophotometry. (B) BZC permeation rate at 24 h (a= films *versus* commercial gel, *= $p < 0.05$).

BZC concentration, the 2.5% FF-MSNs films provided a similar permeation rate as the commercial gel, pointing to the possibility for the development of an effective delivery platform with lower drug concentrations (Figure 5B).

BZC is a local anesthetic widely used for topical anesthesia, but its relatively slow absorption and/or fast biotransformation induces a short duration of action. Due to its application in a variety of dermatological products (gels, creams, ointments and sprays), new topical drug delivery systems have been developed.[35,36] Thus, different materials such as synthetic polymers (carbomer polymers, poly-D,L-lactide-co-glycolide - PLGA, Polyvinyl alcohol, PCL and peptide polymers) have attracted an enormous attention.[35-39]

To our knowledge, this is the first study where the addition of FF-MNTs in PCL has been shown to be an effective strategy for controlling the drug permeation rate with possible skin delivery applications. We note that increasing FF concentration beyond a certain concentration reduces the release time. The optimum release time for the 15% FF-MNTs concentrationsample goes hand-in-hand with the mechanical properties of these fibers; the stress value for this concentration almost reaches saturation. These results suggest that the amount of FF in the matrix could be used as a variable to control the release rate from PCL/FF-MNTs hybrids.

3.5. Biodegradability

The biodegradation of PCL has been investigated against lipase and proteinase-K due to the high efficiency of these enzymes for hydrolysis of polymer chains.[40] For this study, samples were incubated in solution with the enzymes for 25 hours. Figure 6A shows the weight loss of pure PCL and PCL/FF-MNTs scaffolds for different concentrations of FF-MNTs. It is clearly observed that weight loss is strongly impacted by the FF-MNTs concentration. Particularly, we have found that higher degradation rates are found when higher peptide amounts are present in the matrix. The greater weight loss with increase in FF-MNTs concentration could be due to the decreased crystallinity and higher enzymatic affinity towards amide hydrolysis.[28, 41-44] Indeed, diminution of the fraction of ordered domains into the polymer matrix, associated to intercalation of peptide clusters in the interstice of the macromolecular scaffold, likely leads to hydrolysis across the membrane and favours destabilization of the whole polymer structure.[41-44] SEM images obtained after a 25 h degradation period clearly show that increasing FF concentration leads to higher destruction of the fibers. Figures 6B and 6C show, respectively, micrographs obtained before and after degradation process from pure PCL and the 30% FF/PCL. The morphology of the fibers changes drastically for the 30% sample with a clear destruction of the fiber surface. The images of the samples after the biodegradation process for all concentrations are presented in Figure S5. Not only does the addition of FF-MNTs to PCL in the electrospinning process enhance mechanical strength and drug delivery rates, but it also provides a tangible route towards green bio-chemistry.

4. Conclusions

We have presented a simple route for producing hybrid peptide/polymer scaffolds built up from non-covalent conjugation between FF and PCL. The strategy used in this work was based on electrospinning methods, where peptides and polymers are co-solubilizated and submitted to strong electric fields in order to produce fibres with only a few hundred nanometer thicknesses. The structures arising from this procedure have been found suitable for producing homogenous networks and capable for designing polymer membranes potentially usable as skin patches. We have observed that peptides are successfully incorporated into the polymer matrix and self-assemble into micro/nanotubes with remarkable mechanical properties. The elastic behaviour of the composite PCL fibres is strongly affected by peptides and

Journal of Materials Chemistry B Accepted Manuscript

Please do not adjust margins

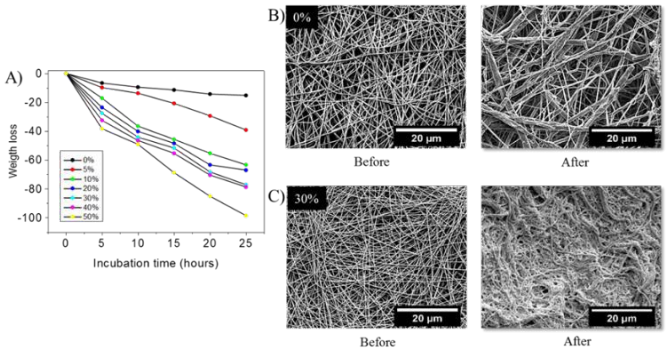

Figure 6. (A) Percentage weight loss for PCL and PCL-FFMNTs composites after 25 hours incubation; (B-C) FEG-SEM of PCL and the 30% FF-MNT sample before and after enzymatic incubation. The biodegradation occurs from the surface to the inside of the fiber.

both DSC and XRPD analyses have shown a close relationship between the mechanical properties and crystalline structure. Specifically, we have found that peptides lead to remarkable loss of crystallinity in the polymer, followed by a brittle-to-ductile transition at the macro-scale. Furthermore, micro-tomography assays have pointed that average pore sizes in the fibers diminish upon increasing the peptide concentration. Unfortunately, the mechanisms as to why these structural changes occur remain somewhat elusive. However, we hypothesize that FF in the interstice of the polymer phase weakens inter-chain interactions and hinders cross-linking across the network, favoring the elastic behaviour of the hybrid material. Also, estimations on entropy changes introduced by mixing peptides to the polymer matrix suggest the growth of disorder and corroborate the break of crystalline ordering indicated by structural assays.

These membranes, exhibiting high flexibility, have been successfully used for modulating the release of benzocaine, an anesthetic widely used in pharmaceutics. It was demonstrated that, on scaffolds containing about 7.5%-30% FF/PCL, release rates are significantly slowed compared to commercially available scaffolds. Interestingly, these same formulations also exhibit the highest elongation limits at break. Finally, we have shown that the scaffolds prepared through this simple strategy are easily degradable upon enzymatic attack; therefore, these biodegradable polymeric matrices have strong potential to behave as a vehicle for sustained release of drugs directly at wound sites.

Acknowledgements

This work was supported by FAPESP (grant no. 2013/12997-0) and CNPq (grant no. 472197/2012-6). INCT in Bioanalytics (FAPESP grant no. 08/57805-2 and CNPq grant no. 573672/2008-3) is kindly acknowledged for grants. M.S.L., S.K.Jr. and E.R.S. acknowledge FAPESP for fellowships (Procs. no.: 2012/15481-1, 2012/01933-8 and 2013/12674-6). LNNano and LNLS staffs are kindly recognized for invaluable help and access to SEM, XRPD and X-ray micro-CT facilities (proposals SEM - 18306, XRD1 - 16150, and Micro CT - 18458). M.S.L. thanks Dr. Ligia Maria Manzine Costa for help on DMA and DSC assays.

References

1. G. Vilar, J. Tulla-Puche and F. Albericio, *Curr Drug Deliv.*, 2012, **9**, 367-394.
2. D. E. Discher and A. Eisenberg, *Science*, 2002, **297**, 967-973.
3. I. W. Hamley, *Biomacromolecules*, 2014, **15**, 1543-1559.
4. T. A. Doll, S. Raman, R. Dey and P. Burkhard, *J. R. Soc. Interface*, 2013, **10**, 20120740.
5. J. Pyun and K. Matyjaszewski, *Chem. Mater.*, 2001, **13**, 3436-3448.
6. V. L. Sedman, L. Adler-Abramovich, S. Allen, E. Gazit and S. J. B. Tendler, *J. Am. Chem. Soc.*, 2006, **128**, 6903-6908.
7. M. Reches and E. Gazit, *Curr. Nanosci.*, 2006, **2**, 105-111.
8. L. Adler-Abramovich, M. Reches, V. L. Sedman, S. Allen, S. J. B. Tendler and E. Gazit, *Langmuir*, 2006, **22**, 1313-1320.
9. G. Zeng, L. Liu, D. Xia, Q. Li, Z. Xin, J. Wang, F. Besenbacher, T. Skrydstrup and M. Dong, *RSC Adv.*, 2014, **4**, 7516-7520.
10. S. Kogikoski Jr, C. P. Souza, M. S. Liberato, T. Andrade Filho, T. Prieto, F. F. Ferreira, A. R. Rocha, S. Guha and W. A. Alves, *Phys. Chem. Chem. Phys.*, 2015, DOI: 10.1039/C5CP07165H.
11. K. Jayaraman, M. Kotaki, Y. Z. Zhang, X. M. Mo and S. Ramakrishna, *J. Nanosci. Nanotechnol.*, 2004, **4**, 52-65.
12. N. Even, L. Adler-Abramovich, L. Buzhansky, H. Dodiuk and E. Gazit, *Small*, 2011, **7**, 1007-1011.
13. D. J. Rubin, H. T. Nia, T. Desire, P. Q. Nguyen, M. Gevelber, C. Ortiz and N. S. Joshi, *Biomacromolecules*, 2013, **14**, 3370-3375.
14. L. W. Chow, A. Armgarth, J.-P. St-Pierre, S. Bertazzo, C. Gentilini, C. Aurisicchio, S. D. McCullen, J. A. M. Steele and M. M. Stevens, *Adv. Healthcare Mater.*, 2014, **3**, 1381-1386.
15. R. F. Silva, D. R. Araujo, E. R. Silva, R. A. Ando and W. A. Alves, *Langmuir*, 2013, **29**, 10205-10212.
16. D. A. Bernards and T. A. Desai, *Adv. Mater.,* 2010, **22**, 2358-2362.
17. M. F. Canbolat, A. Celebioglu and T. Uyar, *Colloids Surf., B*, 2014, **115**, 15-21.
18. B. Wong, S.-H. Teoh and L. Kang, *Drug Deliv. Transl. Res.*, 2012, **2**, 272-283.
19. T. K. Dash and V. B. Konkimalla, *Mol. Pharmaceutics*, 2012, **9**, 2365-2379.
20. M. Chen, Y.-F. Li and F. Besenbacher, *Adv. Healthcare Mater.*, 2014, **3**, 1721-1732.
21. T. K. Dash and V. B. Konkimalla, *J. Controlled Release*, 2012, **158**, 15-33.
22. S. Nicoli, P. Colombo and P. Santi, *AAPS J.*, 2005, **7**, E218-E223.
23. S. V. Fridrikh, J. H. Yu, M. P. Brenner and G. C. Rutledge, *Phys. Rev. Lett.*, 2003, **90**, 144502.
24. A. Mohamed, V. L. Finkenstadt, S. H. Gordon, G. Biresaw, D. E. Palmquist and P. Rayas-Duarte, *J. Appl. Polym. Sci.*, 2008, **110**, 3256-3266.
25. E. Chiellini and R. Solaro, *Adv. Mater.*, 1996, **8**, 305-313.

Journal of Materials Chemistry B Accepted Manuscript

This journal is © The Royal Society of Chemistry 20xx

Please do not adjust margins

26. J. Albuerne, L. Marquez, A. J. Muller, J. M. Raquez, P. Degee, P. Dubois, V. Castelletto and I. W. Hamley, *Macromolecules*, 2003, **36**, 1633-1644.
27. H. Kweon, M. K. Yoo, I. K. Park, T. H. Kim, H. C. Lee, H.-S. Lee, J.-S. Oh, T. Akaike and C.-S. Cho, *Biomaterials*, 2003, **24**, 801-808.
28. J. Ryu and C. B. Park, *Biotechnol. Bioeng.*, 2010, **105**, 221-230.
29. M. I. Souza, E. R. Silva, Y. M. Jaques, F. F. Ferreira, E. E. Fileti and W. A. Alves, *J. Pept. Sci.*, 2014, 20, 554-562.
30. N. Amdursky, P. Beker, I. Koren, B. Bank-Srour, E. Mishina, S. Semin, T. Rasing, Y. Rosenberg, Z. Barkay, E. Gazit and G. Rosenman, *Biomacromolecules*, 2011, **12**, 1349-1354.
31. H. Bittiger, Marchess.Rh and W. D. Niegisch, *Acta Crystallogr., Sect. B: Struct. Sci.*, 1970, **B26**, 1923-1927.
32. L. E. Alexander, *X-ray diffraction methods in polymer science*, Wiley-Interscience, New York, 1969.
33. A. W. Martinez, J. M. Caves, S. Ravi, W. Li and E. L. Chaikof, *Acta Biomater.*, 2014, **10**, 26-33.
34. V. Thomas, M. V. Jose, S. Chowdhury, J. F. Sullivan, D. R. Dean and Y. K. Vohra, *J. Biomater. Sci., Polym. Ed.*, 2006, **17**, 969-984.
35. D. R. Araujo, C. Padula, C. M. Saia Cereda, G. R. Tofoli, R. B. Brito, Jr., E. de Paula, S. Nicoli and P. Santi, *Pharm. Res.*, 2010, **27**, 1677-1686.
36. D. R. Araujo, D. C. Silva, R. M. Barbosa, M. Franz-Montan, C. M. S. Cereda, C. Padula, P. Santi and E. Paula, *Expert Opin. Drug Deliv.*, 2013, **10**, 1551-1563.
37. B. Jeong, S. W. Kim and Y. H. Bae, *Adv. Drug Delivery Rev.*, 2002, **54**, 37-51.
38. C. Padula, A. Fulgoni and P. Santi, *Skin Res. Technol.*, 2010, **16**, 125-130.
39. C. Padula, C. Chiapponi, M. T. Dibari, A. Deriu, F. Sonvico, S. Barbieri, J. Ollivier and P. Santi, *J. Pharm. Sci.*, 2010, **99**, 4277-4284.
40. H. Tsuji, Y. Kidokoro and M. Mochizuki, *Macromol. Mater. Eng.*, 2006, **291**, 1245-1254.
41. S. Khanra, T. Cipriano, T. Lam, T. A. White, E. E. Fileti, W. A. Alves and S. Guha, *Adv. Mater. Interfaces*, 2015, **2**, 1500265.
42. M. J. Jenkins and K. L. Harrison, *Polym. Adv. Technol.*, 2008, **19**, 1901-1906.
43. H. Cai, V. Dave, R. A. Gross and S. P. McCarthy, *J. Polym. Sci., Part B: Polym. Phys.*, 1996, **34**, 2701-2708.
44. M. Reches and E. Gazit, *Science*, 2003, **300**, 625-627.

Journal of Materials Chemistry B Accepted Manuscript

TOC ENTRY

In this work, we design an inedited peptide-based composite built up from the conjugation between micro/nanotubes of L,L-diphenylalanine (FF-MNTs) and polycaprolactone (PCL). The structures arising from this procedure have been found suitable for producing homogenous networks and capable for designing polymer membranes potentially usable as skin patches.

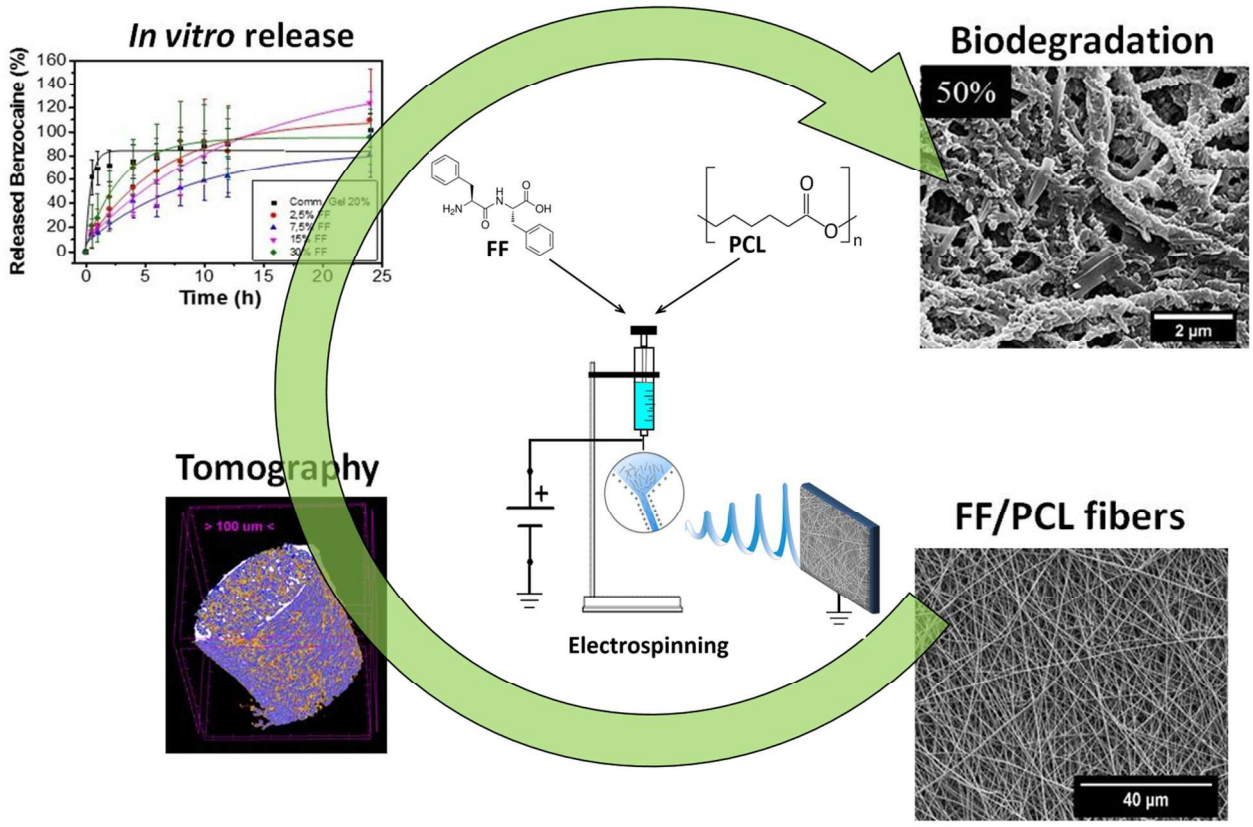

Journal of Materials Chemistry B Accepted Manuscript